International Journal of Computer Information Systems and Industrial Management Applications (IJCISIM)
ISSN: 2150-7988 Vol.3 (2011), pp.019-025
http://www.mirlabs.org/ijcisim

Morphological Analysis and Reconstruction for Computed Tomography

V.E. Asadchikov[1], A.I. Chulichkov[2], A.V. Buzmakov[1], M.V. Chukalina[3], D.P. Nikolaev[4], R.A. Senin[1] and G. Schaefer[5]

[1]*Institute of Crystallography, Russian Academy of Sciences, Moscow, Russia*
[2]*Moscow State University, Moscow, Russia*
[3]*Institute of Microelectronics Technology, Russian Academy of Sciences, Chernogolovka, Russia*
[4]*Institute for Information Transmission Problems, Russian Academy of Sciences, Moscow, Russia*
[5]*Department of Computer Science, Loughborough University, Loughborough, U.K.*

Abstract

Image reconstruction is an important task in X-ray computed tomography. In this paper we discuss the results of morphological analysis of test objects in high-noise conditions and compare image reconstruction using two widely employed methods in computed tomography, namely Filtered Back Projection and Algebraic Reconstruction Technique. In our test tomography experiments, we used a laboratory X-ray source designed and manufactured at the Institute of Crystallography, Moscow, Russia.

1. Introduction

This work is devoted to the problem of image reconstruction [1-7] and morphological analysis of images in X-ray computed tomography (CT). A key problem here is image reconstruction from the distribution of linear attenuation coefficients inside the object under study. In medical applications, it is often more important to determine only the parameters of inclusions, such as their size, position, etc. with some controlled accuracy. This can be done by performing morphological analysis [8, 9].

2. Test object

A polypropylene vial, 10.5 mm in diameter and with 1.6 mm wall thickness, filled with water was used as a test object. This is a classical test object widely employed for calibration of medical tomographs and is convenient because it is comprised of two distinctly separated homogeneous media. The vial diameter and composition/thickness of its walls can be adjusted in such a way that the absorption of a given X-ray is significant at a relatively high transmission, which in turn would ensure an image contrast at a level of several dozen percent. In our experiments, the vial was illuminated by X-rays (Mo-Kα radiation,. λ=0.07 nm) in parallel [5, 6] scan mode.

3. Image reconstruction

In the following we describe the mathematical model we used for image reconstruction. Assume that the test object is illuminated with a beam of intensity I_0. Let $f(x,y)$ be the distribution of the attenuation coefficient in the plane of the scanned phantom section and φ be the rotation angle of beam incidence. At separation ξ from the origin of co-ordinates, an infinitely thin X-ray beam can be described by (see also Figure 1)

$$x\cos\varphi + y\sin\varphi = \xi \quad (1)$$

If the channel width of the position-sensitive detector is infinitely small, the recorded signal can be represented as

$$I(\varphi,\xi) = I_0 \exp(-\int f(x,y)\delta(x\cos\varphi + y\sin\varphi - \xi)dxdy) \quad (2)$$

where δ is the Dirac delta function.

Introducing a new function, this expression can be rewritten in the following form:

$$p(\varphi,\xi) = \ln\left(\frac{I_0}{I(\varphi,\xi)}\right) = \iint f(x,y)\delta(x\cos\varphi + y\sin\varphi - \xi)dxdy \quad (3)$$

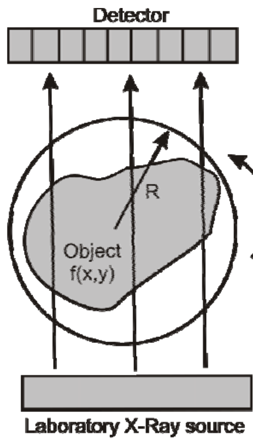

Figure 1. Scheme of laboratory X-ray microtomograph.

The transformation that converts the object function *f(x,y)* into the projection function *p(φ,ξ)* is termed the Radon transformation [10]. The reconstruction of an image (distribution of linear attenuation coefficient) from a set of recorded projections is a classical problem in tomography [5,6] and is typically being solved using either integral (e.g. filtered back-propagation (FBP)) or algebraic (ART) methods. In this paper, we present a comparison of the results obtained by these two methods and describe a morphological approach to evaluate the shape parameters of investigated object inclusions.

4. Shape parameters of inclusions: morphological approach

The function $f(x,y)$ is defined by the vial shape. It is a stepwise function which takes on value c_1 outside of the circle that represents the external boundary of the vial, is equal to c_2 between the walls of the vial, and equals c_3 inside the circle of the internal boundary. This can be expressed as

$$f(x,y)=\sum_{i=1}^{3} c_i \chi_i(x,y)\,. \tag{4}$$

where the functions $\chi_i(x,y)$ are equal to 1 at points (*x,y*) where $f(x,y)=c_i$ and are 0 otherwise. The set of linear combinations $\chi_i(x,y)$, *i*=1,2,3, forms a 3-dimensional linear sub-space of all functions. The sub-space kind is defined by four numerical parameters (x_0,y_0,d_1,d_2) describing the centre co-ordinates and circle diameters of the vial.

Having substituted Equation (4) into Equation (3), we obtain that $p(\varphi,\xi)$ is an element of the 3-dimensional sub-space $V_3(x_0,y_0,d_1,d_2)$. This sub-space originates from the linear combinations of the functions obtained by integration of $\chi_i(x,y)$ multiplied by the delta function. This kind of sub-space is also defined by (x_0,y_0,d_1,d_2) .

Let's choose these parameters so that the results of the projection measure $p(\varphi,\xi)$ are as close as possible to the sub-space. We define the morphological distance from the function $p(\varphi,\xi)$ to $V_3(x_0,y_0,d_1,d_2)$ by a fractional value whose numerator is the Euclidean distance $\rho(V_3(x_0,y_0,d_1,d_2),p)$ from $p(\varphi,\xi)$ to $V_3(x_0,y_0,d_1,d_2)$ and whose denominator is the distance $\rho(V_0,p)$ from $p(\varphi,\xi)$ to the set V_0 of functions that are constant [7-8]:

$$j_{(x_0,y_0,d_1,d_2)}(p)=\rho(V_3(x_0,y_0,d_1,d_2),p)\big/\rho(V_0,p) \tag{5}$$

The denominator is discarded when $p(\varphi,\xi)=\mathrm{const}$ which corresponds to measurements of a projection of homogeneous space. Such a projection is formally is described by

$$c_1=c_2=c_3 \tag{6}$$

In the presence of a casual error of measurement $p(\varphi,\xi)$ morphological affinity is not equal to 0 with a probability of 1. If the noise is Gaussian, then $j_{(x_0,y_0,d_1,d_2)}(p)$ is a random variable with the distribution depending on parameters (x_0,y_0,d_1,d_2) .

The value $j_{(x_0,y_0,d_1,d_2)}(p)$ is a measure of similarity of the given measurements with theoretically calculated data from the vial with (x_0,y_0,d_1,d_2). It is the noise to signal ratio provided that x_0,y_0,d_1,d_2 are the true values of shape parameters of the vial. If this condition is met then the difference of the numerator $\rho(V_3(x_0,y_0,d_1,d_2),p)$ from 0 can be explained only by the presence of noise. The denominator represents the difference of projection from the constant of its best approximation and characterises the projection part, bearing information about the parameters of the vial.

A point estimate of (x_0,y_0,d_1,d_2) can be obtained using a solution to the following variation problem:

$$j_{(x_0,y_0,d_1,d_2)}(p)\rightarrow \min_{x_0,y_0,d_1,d_2}\,. \tag{7}$$

For our test object, the minimum of $j_{(x_0,y_0,d_1,d_2)}(p)$ was attained at the inner vial diameter about 7.8 mm and outer diameter 10.5 mm, which agrees well with the size of the test object used in the experiments.

According to [11], the set which can be used to evaluate parameters (x_0,y_0,d_1,d_2) with probability α has the form:

$$\Psi_\alpha(p)=\left\{(x_0,y_0,d_1,d_2): j_{(x_0,y_0,d_1,d_2)}(p)\le c_\alpha\right\} \tag{8}$$

A diagram of the function $j_{(x_0,y_0,d_1,d_2)}(p)$ of co-ordinates of the vial centre at fixed values of diameters d_1, d_2 is shown in Fig. 2.

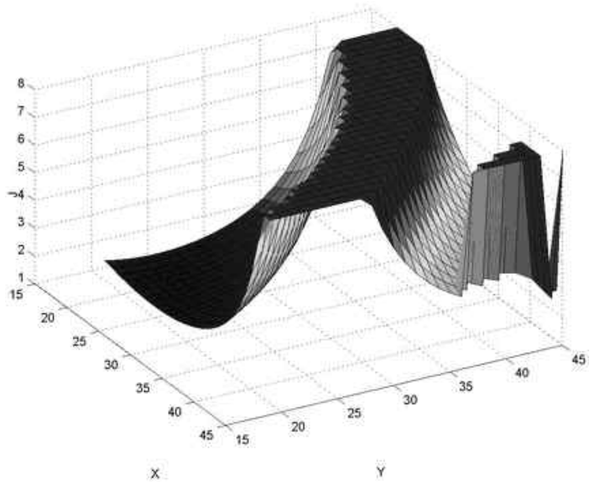

Figure 2. Function $j_{(x_0,y_0,d_1,d_2)}(p)$ of co-ordinates of vial centre at fixed values of diameters d_1, d_2.

Setting the value of noise to signal ratio, we will receive set of points $\{(x_0, y_0, d_1, d_2)\}$, that give the position of the vial centre. It is the set of points, for which diagram lays been lower than chosen value.

5. Filtered back-projection method

This method is most frequently being used in medical tomography [1,5]. It is based on a projection theorem according to which the Fourier transform of projection data along coordinate ξ,

$$P(\varphi,\omega) = \int p(\varphi,\xi) e^{-i\omega\xi} d\xi = \iint f(x,y)\exp(-i(\omega x\cos\varphi + \omega y \sin\varphi))dxdy \quad (9)$$

is equivalent to the Fourier transform of the object function in polar co-ordinates

$$F(\omega_x,\omega_y) = \iint f(x,y)\exp(-i(\omega_x x + \omega_y y))dxdy \quad (10)$$

i.e.

$$P(\varphi,\omega) = F(\omega_x,\omega_y) \quad (11)$$

For reconstruction of image *f(x,y)*, one has to perform the reverse Fourier transform of *P(φ,ω)*

$$f(x,y) = \iint \Phi(\omega) P(\varphi,\omega) e^{i\omega\xi} d\omega d\varphi \quad (12)$$

where *Φ(ω)* is the function of the frequency filter.

For a parallel measurement scheme

$$\Phi(\omega) = \begin{cases} \omega_{\max} - \varepsilon|\omega| & \text{if } |\omega| \le \omega_{\max} \\ 0 & \text{otherwise} \end{cases} \quad (13)$$

where $\omega_{\max} = (2T_d)^{-1}$ is the maximal sampling rate, T_d the linear size of detector array element, and $\varepsilon \in [0,1]$ some parameter.

In practice [1,5,6], Equation (12) can be solved using the filtered backprojection (FBP) method. Let *Φ(ω)* be given by Equation (13) and *K(ξ)* be its Fourier transform, then the product of *Φ(ω)* and the Fourier transform of projection can be regarded as the Fourier transform of the convolution of projection with function *K(ξ)*:

$$f(x,y) = \iint K(\xi - \xi_0) p(\varphi,\xi) d\xi d\varphi \quad (14)$$

where $\xi_0 = x\cos\varphi + y\sin\varphi$ and

$$K(\xi) = \int |\omega| e^{i\omega\xi} d\omega = \frac{1}{2T_d}\frac{\sin(2\pi\xi/2T_d)}{2\pi\xi/2T_d} - \frac{1}{4T_d^2}\left(\frac{\sin(\pi\xi/2T_d}{\pi\xi/2T_d}\right)^2 \quad (15)$$

A sample FBP reconstruction is shown in Figure 3(a). Shown in Figure 3(b) are cross-sections obtained by FBP and by a modified ART method introduced in the following section.

Integral calculation is performed using a numerical method. Conveniently, data processing can occur almost in parallel with measurement, since the calculation of a return projection after a filtration can be performed during registration of the following projection, and the result of the calculation summarised in appropriate storage locations.

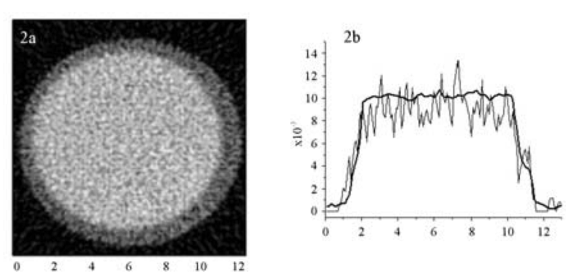

Figure 3. a) Section of polypropylene tubes with water reconstructed by FBP. Average rate of absorption - water: μ= 0094 mm^{-1}, σ^2=1.5·10^{-4}; polypropylene: μ=0056 mm^{-1}, σ^2=0.6·10^{-4}, b) Cross-section of the reconstructed image. Gray line: FBP reconstruction; black line (smooth): ART reconstruction with median filtering, γ=0.005.

Before the real experiment, mathematical simulation has been performed to estimate the optimal conditions. To reach the optimum here means to reduce the time of experiment performance, and to keep acceptable quality of the reconstruction. The FBP technique was used for condition estimation. Understandably, the structure of liquid, at scales comparable with resolution of the device, is homogeneous and constant in terms of density. Hence, disorder values in terms of fluid density, and also average value of density received during the experiment can characterise the accuracy of the method of measurement and reconstruction.

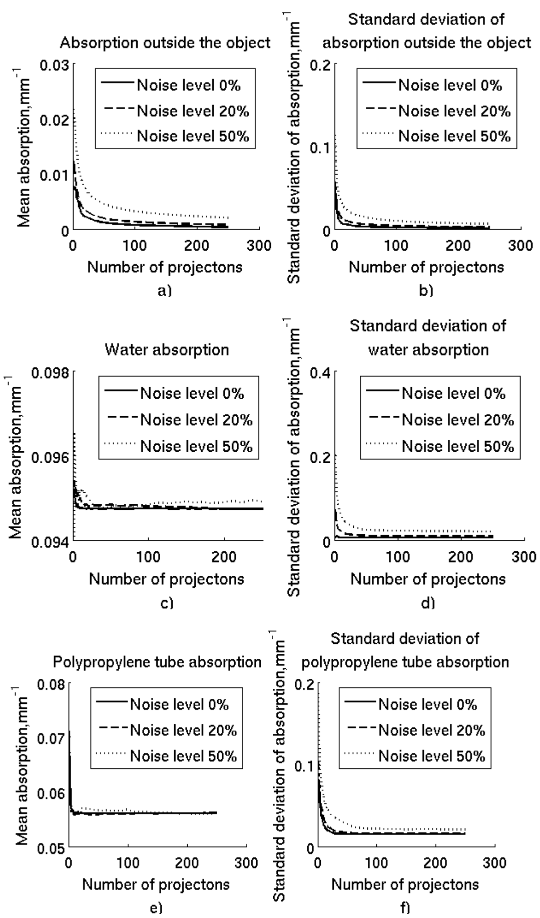

Figure 4. Absorption and standard deviation depending on number of projections, used for reconstruction, for different noise levels and different parts of the object (a,b – outside of object; c,d – water; e,f – polipropilen tube).

The simulation parameters were as follows:-

- the size of the reconstructed region (size of slice) is 250x250 pixels;
- pixel size is 0.1x0.1 mm^2;
- the vial is presented by a cycle with an external diameter of 104 pixels and an internal diameter is 88 pixels;
- the linear attenuation coefficient in the wall of vial is 0.006 $pixel^{-1}$, linear attenuation coefficient inside the vial is 0.01 $pixel^{-1}$;
- the simulated projections were distorted with additive noise, having normal distribution.

Figure 4 shows, how quickly and to what value the reconstructed value converges when increasing the number of projections and at different levels noisiness of the original signal. At noise levels of less than 30% and number of projections of more than 70 (these conditions correspond to the real experiment) the intensity of artefacts does not exceed 0.002 mm^{-1}, which makes about 5% of the tabulated value of linear absorption coefficient of the object under study.

The observed dependencies show that 72 projections measured during the experiment is sufficient so as to obtain the correct reconstructed value with an accuracy about 5%. Underestimated values of are due the frequency filtering method used in reconstruction by FBP. Hence this part of the signal energy is diffused.

6. Modified ART method

In this method, an image to be reconstructed is covered by a grid comprising of N pixels. For the j-th pixel, the function f_j is assumed to be constant. Then the integral Equation (3) can be reduced to the following system of linear algebraic equations:

$$p_i = (f, t_i), \quad i = 1, \ldots, M \qquad (16)$$

where the i-th component of vector t_i is regarded as the weighting coefficient which, in the model of infinitely thin beams [12], is the path length of an X-ray beam passing through the j-th pixel, and M is the total number of points in all recorded projections, i.e. the product of the number of projection angles M_φ and array elements in the position-sensitive detector).

Equation (4) is solved using the iteration method [13]. For each iteration k, there is a solution f^k which is improved upon by the projection of vector

$$f^{k+1} = f^k + \gamma \frac{p_i - (f^k, t_i)}{(t_i, t_i)} t_i \qquad (17)$$

on the i-th hyperplane defined by equations from (16). Here, γ is the relaxation parameter [14].

In our implementation of the algorithm we first calculate a set of weight sparse matrices t_i for all rotation angles.

In many ART implementations the weights are simply replaced by 1s and 0s depending on whether the centre of the pixel is within the fine ray. This makes the implementation easier. This approximation, although easy to implement, often leads to artefacts in the reconstructed images. In our calculations, we used the beam–strip model [12]. The weighting coefficient was calculated as the ratio of pixel area hit by the beam to the overall pixel area. The beam diameter was chosen equal to the size of detector array element.

An iteration is assumed completed when projection onto all hyperplanes has been performed. The choice of path tracing represents a standalone problem [15].

To minimise the influence of two neighbouring hyperplanes on each other we used the following scheme:

$$\begin{gathered} p(\varphi_1,\xi_1), p(\varphi_1+\frac{\pi}{2},\xi_1), p(\varphi_1,\xi_2), p(\varphi_1+\frac{\pi}{2},\xi_2),..., \\ p(\varphi_1+\frac{\pi}{2},\xi_{N/2}), p(\varphi_1,\xi_{N/2}),..., p(\varphi_M+\frac{\pi}{2},\xi_{N/2}) \end{gathered} \quad (18)$$

Because the projections are noisy, the intersection of the hyperplanes is not a point in the *N*-dimensional space but a polygon. Each iteration projects the estimated solution to a polygon wall area. On the other hand, the solution sought for belongs to the image class sub-space. The size, shape and position of the sub-space depend on the accuracy of the image description (accuracy of the image model). The image sub-space and the polygon can intersect or be close to each other. The regularisation operator brings the estimated solution from the polygon wall area to the image sub-space [16]. The space of the piecewise constant functions is well suited for the description of the tomography images. However, it is very difficult to construct the projector which brings an estimated solution to this image sub-space. We have taken the space of piecewise smooth functions as the image space, i.e. if the function belongs to this space it will belong to the same space after the median operator was implemented. Then the median filtering operator can be used as the projector from the polygon wall area to the image sub-space. We have implemented the median filtering as the second sub-iteration [17,18].

The non-negativity constraint is reinforced, when instead of f<0 we set f=0.

One iteration is completed after the full set of measurements has been processed.

In the next iteration it is projected onto the hyperplane represented by the first Equation in (16), and successively onto the rest of the hyperplanes in Equation (16), then the filtering is implemented and so on until the last iteration.

In the last iteration, all images are saved. The final step of the algorithm is the averaging over these images to exclude the specific influence of the last hyperplane projection.

The initial guess f^0 is assigned a value of zero. It was shown [19] that from any initial guess the sequence generated by the ART converges to a weighted least square solution. This initial guess is projected on the hyperplane represented by the first Equation in (16) to yield $\vec{f}_1^{\,0}$. The subscript indicates how many hyperplanes are included in the correction process. After each projection onto a hyperplane, the estimated image is updated. The first sub-iteration is finished if the correction over all hyperplanes is finished.

The results are presented in Figure 5. For water, μ=0.098 mm^{-1}, σ=0.003 mm^{-1}. On 2xAMD Opteron 275 computer (RAM 8 Gb), the reconstruction time for the 2D image was 4 s.

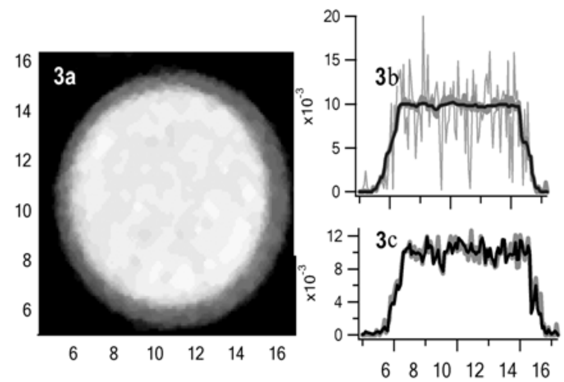

Figure 5. a) Result of the reconstruction by ART. Used parameters: γ=0.01; median filtering mask is 3x3 pixels.
b) Cross-section of the reconstructed image. Gray line: reconstruction without median filtering, γ=0; black line: reconstruction with median filtering, γ=0.005.
c) Cross-section of the reconstructed image. Gray line: median filtering mask is 3x3, γ=0; black line: γ=0.03, reconstruction without median filtering.

7. Conclusions

In this paper we have performed image reconstruction using two different methods. In conditions of high noise, each of the methods has its own advantages. FBP provides better reconstruction of boundaries, ART shows lower dispersion upon reconstruction within prolonged areas, while morphological analysis is better in reconstruction of inclusions. A new modified version of ART was used in our experiments and shown to give good results. Currently, we are planning to perform rapid image reconstruction by combining the above methods.

Acknowledgements

This work was partly supported by RFBR (09-07-00473-a, 08-07-00120, 09-02-12251-ofi_m, 09-02-

12210_ofi_m, 08-01-00802a), PICS 3470, ISTC 3124, the program “Fundamental science to medicine”. The work of M. Chukalina was partly supported by the Institute of Crystallography by A.V. Shubnikov RAS.

References

[1] Kalender V., Computed tomography.-The basis, technology, the quality ot the image in the sphere of the clinical use, Tehnosfera, 2006.

[2] De Clerck N., Meurrens K., Weiler H. *et al.* “High-Resolution X-ray Microtomography for the Detection of Lung Tumors in Living Mice”, *Neoplasia*. 6(4), 2004, pp. 374–379.

[3] Asadchikov.V.E., Babak V.V., Buzmakov A.V. *et al.* “X-ray diffractometer with moving system source-detector”, *Devices and the technology of the experiment*, 3, 2005, pp. 99-107.

[4] Asadchikov V.E., A.V. Buzmakov, A.V. Popov, R.A. Senin ,I.V. Suloev, A.V.Vinogradov, “Xray magnification with the use of the microcapillary lens: simulations and experiments”, *Optical Technologies in Biophysics and Medicine VII: Proc. SPIE*, 2005, pp. 61631-61634.

[5] Kak A.C., Slaney M., *Principles of Computerized Tomographic imaging*. N.Y.: IEEE Press, 1988.

[6] Natter F., *Mathematical aspects of the computer tomography*, Mir, 1990.

[7] Senin R. A. , Buzmakov A.V., Konovko A.V., Smirnov I.S., Geranin A.S. and Asadchikov V.E., "Gain in spatial resolution of X-ray laboratory microtomographs with enlarging X-ray optical elements", *Journal of Physics: Conference Series*, 186, 2009, 012035, pp. 1-3.

[8] Pyt’ev Y.P., *Problems of the mathematical analysis of the images*, Science, 1984.

[9] Chulichkov A.I. “Sets, valuing parameter of waveform” *Intellectual systems and computer sciences: Info IX International Conference*, MSU, 2006, pp. 310.

[10] Radon J., "Über die Bestimmung von Funktionen durch ihre Integralwerte längs gewisser Mannigfaltigkeiten", *Berichte über die Verhandlungen der Sächsische Akademie der Wissenschaften (Reports on the proceedings of the Saxony Academy of Science)*, 69, 1917, pp. 262-277.

[11] Pyt’ev Y.P., Chulichkov A.I., “Morphological image analysis: Results and prospects”, *Mathematical methods of the identification of the images : Proc. of the 12-th Russian Conf.*, MAX Press, 2005, pp. 416-419.

[12] Chukalina M., Buzmakov A., Senin R., Asadchikov, “X-ray tomography: artifacts reasons”, *Proceedings of the Nanophysiscs and nanoelectronics Symposium. Nizhnii Novgorod, Russia, March 25-29*, 2005, pp. 294-295.

[13] Gordon R., “A tutorial on ART (algebraic reconstruction technique)”, *IEEE Trans. Nuclear Science,* 21, 1974, pp. 78-93.

[14] Censor Y., Eggermont P. B. P., Gordon D., “Strong underrelaxation in Kaczmarz's method for inconsistent systems”, *Numerische Mathematik*. 41(1), 1983, pp. 83-92.

[15] Guan H., Gordon R. Yu. Zhu, “Combining various projection access schemes with the algebraic reconstruction technique for low-contrast detection in computed tomography”, *Phys. Med. Biol.* 41, 1998, pp. 2413-2421.

[16] Cheremuhin E., A.I. Chulichkov, “Usage of the measurement computer systems in tomography”, *Issue of Calc. Math. and Math. Phys.* 45, no.4, 2005, pp.741-752.

[17] Davidsov J.L., Ch. A. Garcia-Stewart, K.B. Ozanyan, P. Wright, S. Pegrum, H. McCann, (2006) “Image reconstruction for chemical species tomography with inregular and sparse beam array”, *Proceedings of Photon 06.*

[18] Chukalina M., Nikolaev D., Simionovici A. (2007) “ART in X-ray tomography: image noise reduction”, European Conference on Modelling and Simulation, 309-312.

[19] Ming J., W. Ge, “Convergence of the simultaneous algebraic reconstruction technique (SART)”, *IEEE Trans. Image Processing*, 12, no.8, 2004, pp.957-961.

VICTOR E. ASADCHIKOV received his PhD in Physics at the Institute of Crystallography RAS. He is Head of Laboratory of X-ray Reflectivity and Neutronography. His research interests include x-ray tomography and diffraction.

ALEXEY I. CHULICHKOV received his Doctor in Physics and Mathematics degree at Moscow State University in 1993, and became Professor of the Physics Faculty of the Moscow State University in 1994. His main scientific interests include mathematical modelling of physical systems and measuring processes, mathematical problems in the measuring analysis, planning and interpretation, and image processing.

ALEXEY V. BUZMAKOV received his PhD degree at Moscow State University in 2009 in Physics. He has been a research scientist at the Institute of Crystallography RAS since 2006. His research activities are in the areas of digital image processing, x-ray optics and microtomography.

MARINA V. CHUKALINA received her PhD in Physics at the Institute of Microelectronics Techlogy RAS where she has been working since 1988. Her interests include the development of signal and image processing tools for X-ray Microscopy and Tomography.

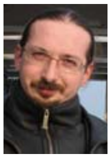

DMITRY P. NIKOLAEV received his PhD degree at Moscow State University in 2004 in Physics. He has been a research scientist at the Institute for Information Transmission Problems RAS since 2000. Now he is a head of Sector for Modeling of Visual Systems. His research activities are in the areas of computer vision with primary application to colour image understanding.

ROMAN A. SENIN received his PhD in Physics in 2005 at the Institute of Crystallography RAS. He has been a research scientist at the Kurchatov Center of Synchrotron Radiation since 2008. His research activities are in the areas of x-ray imaging and microtomography.

GERALD SCHAEFER received his PhD in Computer Vision from the University in East Anglia. He is currently working in the Department of Computer Science at Loughborough University. His research interests include computer vision, colour image analysis, medical imaging, and computational intelligence.